Assessment of spectral UV radiation at Marambio Base, Antarctic Peninsula

Klára Čížková[1,2], Kamil Láska[1], Ladislav Metelka[2], Martin Staněk[2]

[1]Department of Geography, Faculty of Science, Masaryk University, Brno, 611 37, Czech Republic
5   [2]Solar and Ozone Observatory, Czech Hydrometeorological Institute, Hradec Králové, 500 08, Czech Republic

Correspondence to: Klára Čížková (cizkova.klara@mail.muni.cz)

Abstract. This study aims to assess response of spectral UV radiation to different atmospheric and terrestrial factors, including solar zenith angle, ozone, and cloud cover and albedo, in southern polar environment. For this purpose, 23260 individual unique spectra (300–363 nm), obtained by the B199 Mk-III Brewer spectrophotometer at Marambio Base, Antarctic Peninsula
10   Region, over the period 2010–2020, were studied. A neural network model was developed to investigate the effects of the explanatory variables at individual127 wavelengths in the interval 300–363 nm, with the resolution of 0.5 nm. SZA proved to be the most important parameter, followed by cloud cover, TOC, and surface albedo. The relative SZA effect is greatest at the shortest wavelengths, where a 1° decline in SZA results in a 6–18 % increase in UV irradiance (305 nm). Also TOC affects particularly the short wavelengths, while at 305 nm, a 10 DU decrease in TOC causes a 7–13 % increase in UV irradiance. In
15   some seasonsThe large-scale ozone holes (e.g., in 2011–2012, 2014–2015, 2018–2019), the large-scale ozone holes) caused the UV irradiance at very short wavelengths peak in spring, whereas in other seasons (e.g., 2010–2011, 2012–2013), the maxima at all wavelengths were recorded in summer. (November to January). Absorption of UV radiance by ozone affected also the temporal distribution of very high UV irradiances, while at 305 nm, they were observed both in spring and summer months, and at 340 nm, they occurred mostly in summer. The effect of cloud cover was strongest near the fully cloudy sky,
20   and in summer months. Albedo affected the UV irradiance only weakly, its effect was strongest in early spring and late fall, when the Antarctic clouds tend to be thickest.

1 Introduction

Solar UV radiation has been a source of scientific interest since its discovery in 1801. The biological effects of UV radiation, such as its erythemal effects in humans, have beenwere first described in the late 19th century, followed by the thorough
25   medical research in the 20th century (Diffey, 1980). Since then, many biological effects have been accounted to UV radiation. Amongst them are, for example, melanin production, skin wrinkling, protein damage, or even the alterations of DNA structure in humans and other organisms, which may lead to melanoma (e.g., Czerwińska and Krzyścin, 2019; Holick, 2016). On the contrary, the exposure to solar UV irradiance catalyzescatalyses vitamin D creation, which is essential for musculoskeletal health, and may even lead to the lowering of blood pressure in humans (Young et al., 2021). Of course, the effects of UV

30   irradiance are not only limited to humans and other higher organisms. An increased exposure to UV irradiance may also lead to, for example, the reduction of terrestrial plant productivity, or the inhibition of unicellular organisms, both terrestrial and aquatic (~~UNEP, 2010~~Barnes et al., 2022).

As stratospheric ozone is the most important gas affecting the absorption of UV radiation in the atmosphere, preventing as much as 97–99 % of incident short-wavelength UV irradiance (e.g., Jovanović et al., 2019, McKenzie et al., 2007), UV

35   radiation research received the greatest attention after the discovery of the Antarctic ozone hole in the 1980s (Chubachi, 1985; Farman et al., 1985). Since then, many events have taken place to eliminate the ozone depletion, most notably the 1987 Montreal Protocol and its numerous amendments (Jovanović et al., 2019). The recent positive stratospheric ozone trends in southern polar regions, when for example in September, TOC was reported to grow significantly at rates between 1.8 and 2.8 DU per year (e.g., McKenzie et al., 2019; Pazmiño et al., 2018; Solomon et al., 2016), contributed to a decrease in UV

40   irradiance recorded at various Antarctic sites (Bernhard and Stierle, 2020). However, ozone hole still keeps forming each Antarctic spring, increasing the UV irradiances and threatening the rare Antarctic ecosystems (e.g., Cordero et al., 2022). UV radiation assessment is, therefore, still an important scientific task in both hemispheres, including for example the Arctic ozone loss in spring 2020 (e.g., Bognar et al., 2021).

The solar UV spectrum is commonly divided into three bands: UVC (200–290 nm), which is almost entirely absorbed in the

45   atmosphere, UVB (290–320 nm), and UVA (320–400 nm), which is the least photobiologically active. However, this division is semi-arbitrary, and there is no clear transition between UVA and UVB bands, as it is illustrated even by the possible division at 315 nm (Diffey, 1990; Juzeniene et al., 2011). Despite this rather simple division, the precise shape of the solar UV spectrum is far more complex. It is given mostly by the incident solar irradiance at the top of the atmosphere and the wavelength-dependent absorption of UV irradiance by various atmospheric gases (e.g., Kerr and Fioletov, 2008). The extraterrestrial solar

50   spectrum has long been described, and the strong absorption at certain wavelengths has been explained by the Fraunhofer lines, for example the strong Fe line at about 358 nm or the NH line at 336 nm (Stair, 1951). The major atmospheric absorbers in the UVB region are ozone, nitrogen dioxide and ~~sulfur~~sulphur dioxide, but due to their respective abundance, ozone reduces the surface UV irradiance 200 to 300 times more than the other two (DeLuisi, 1997). The UVB region is mostly affected by the Huggins absorption band, which spreads between approximately 310 and 370 nm and exhibits a sequence of wave-like

55   structures (Qu et al., 2004).

Spectral UV observations require a quality instrument with high sensitivity, satisfactory wavelength resolution and precise stray light rejection (Webb, 1991). Such instruments only became available in the 1990s. Since then, the solar UV spectra have been monitored at various locations already for several decades (e.g., McKenzie et al., 1993; Webb, 1991), especially after the introduction of the double monochromator Brewer Mk-III spectrophotometer (Bais, 1997). However, the assessment of

60   spectral solar UV irradiance in the Antarctic remains quite rare, especially without further processing. In most studies from Antarctica, UV irradiance is integrated using various action spectra, most commonly the UV Index or the erythemal action spectrum, or several selected wavelengths or their intervals are evaluated. So far, the entire solar UV spectrum has been mentioned only in few instances, such as the case studies from Union Glacier Camp by Cordero et al. (2014) or Escudero

Station by Cordero et al. (2013). However, the above-mentioned studies only included short observation campaigns, so a complex evaluation of long time series of solar UV irradiance spectra from Antarctica is still missing.

This study aims to ~~close~~contribute to closing this gap ~~and to assess~~by assessing the 10 year long time series of spectral UV irradiances recorded at Marambio Base in the Antarctic Peninsula region. We focused on UV climatology and year to year differences, extreme values, as well as on the factors affecting the UV irradiance at individual wavelengths. We studied the effects of solar zenith angle (SZA), total ozone column (TOC), and cloud cover ~~and albedo~~ using artificial neural network modelling (ANN), which allowed us to focus on key factor and linkages between the southern polar vortex and UV irradiance reaching the Antarctic continent. The paper is organized in two main sections: Section 2 gives the data and methods used in the study, while the study site is specified in Section 2.1, the instrumentation used for solar UV spectral irradiance observation in Section 2.2, and other datasets (SZA, TOC, cloud cover and albedo) are described in Section 2.3. Further on, Section 2.4 states the methods used for data processing and analyses, including the ANN model and its validation., which is further described in Appendix A. Section 3 then gives the results of this study and also compares them in a wider context, while Section 3.1 focuses on the climatology and changes of spectral UV irradiance and the selected explanatory variables, and Section 3.2 presents the effects of the explanatory variables on the spectral UV irradiance as computed through the ANN model. Lastly, Section 4 summarizes the main findings.

2 Materials and Methods

2.1 Study Site

The measurements assessed in this study took place at Marambio Base (S 64.14°, E 56.37°, 196 m a. s. l.). This permanent Argentinean base was founded in 1969 and it is located on the ice-free Seymour Island in the Antarctic Peninsula region. The mean temperature doesn't exceed 0°C in any month, so snow cover, which increases UV radiation reflection, may be present all year long. The cloudiest season is summer, with fog being prevalent especially in December and January (Lakkala et al., 2018; 2020). Marambio Base lies close to the edge of the southern polar vortex (Fig. 1), so during its existence in Antarctic winter and spring, the station lies just inside (about 60 ~~%),~~% of all cases), on the edge, or just outside the vortex (Karhu et al., 2003; Pazmiño et al., 2005).

2.2 Solar UV Spectra

The solar UV spectra have been obtained by the B199 double monochromator Brewer spectrophotometer over the period from February 2010 to January 2020. During this time, the B199 spectrophotometer was operated by the Czech Hydrometeorological Institute (CHMI) and the National Meteorological Service of Argentina. (NMSI). The instrument was serviced each year in January or February by specialists from ~~the Czech Hydrometeorological Institute~~CHMI and International Ozone Services, Inc., Canada. Each year, a calibration has been performed using three to five travel 50W lamps, which were calibrated right before the departure to Marambio Base using the B184 Brewer spectrophotometer in the CHMI Solar and Ozone Observatory in

95 Hradec Králové, and three 1000W lamps S1450, S1451, and S1542 calibrated in the World Radiation Center in Davos. Moreover, in 2012 and 2016, the B199 spectrophotometer was calibrated against the world traveling standard B017 ~~directly at Marambio Base.~~ and spectrally calibrated with the use of HG and CD spectral lamps directly at Marambio Base. The spectrum was calibrated in 2012, 2016, and also in 2019. A final calibration was performed in 2020 both at Marambio and after the instrument returned to Hradec Králové. The yearly calibration results, which were taken in account stepwise, yielded

100 a maximum difference of -7 % in 2014. The mean absolute annual difference in the 2010–2020 period was 4.1 %. The standard lamp ratios R6, R5, and results from Dead time and Run stop test were additional parameters to monitor for checking of the instrument stability. This information was saved in the instrument checklist at the Solar and Ozone Observatory in Hradec Králové.

The B199 spectrophotometer obtains the spectral UV irradiance within the interval 286.5–363.0 nm, where the bandwidth is

105 0.5 nm. However, the very short wavelengths present higher uncertainty due to pronounced atmospheric attenuation and the sensitivity of the instrument itself (Bais, 1997; Bojkov et al., 1995). Moreover, the shortest wavelengths are also strongly absorbed by ozone, which leads to a very weak transmitted information affected by noise and the dark signal of the detector, and an uncertainty exceeding 10 % (Cordero et al., 2008; 2016). Therefore, only the wavelengths longer than 300 nm were used in this study.

110 Over the period of its operation, the B199 spectrophotometer obtained 45 073 solar UV spectra, each of which was quality-checked for spikes~~.~~ (Meinander et al., 2003), and the wavelength shift was ~~analyzed~~analysed based on Fraunhofer lines~~.~~ using the SHICrivm software package (https://www.rivm.nl/en/uv-ozone-layer-and-climate/shicrivm). The 23 260 of the spectra, which had been successfully paired with explanatory variables (see Section 2.3), were used for this study. The temporal distribution of the spectra is shown in Fig. 2. It can be seen there were several data gaps, of which the longest occurred due to

115 a remotely discovered technical failure of the instrument at the end of 2016. This mechanical problem was resolved early in 2017 during the regular maintenance so the measurements could continue.

2.3 Explanatory Variables

Each of the solar UV spectra used in this study has been paired with following explanatory variables: solar zenith angle (SZA), measured during each of the B199 spectral observations, total ozone column (TOC), cloud cover, and albedo. According to

120 Petkov et al~~.,~~. (2016~~,~~). these belong to the most important variables affecting UV irradiance at the nearby Mendel Station.

The TOC values used in this study have also been acquired by the B199 Brewer spectrophotometer. Due to their very high precision, which can reach up to 0.15 % (Scarnato et al., 2010), only the Direct Sun measurements have been taken in account. The solar UV spectra have been paired with these independent TOC observations, while only the TOC values within 60 minutes from the spectral measurements have been used. Therefore, more solar spectra could be matched with the same TOC

125 measurement, provided it was taken within the 60 minute time distance and it was the closest observation. When there was no match of the spectrum with a Direct Sun TOC measurement within the specified time interval, the spectrum was removed from the dataset. The 60 minute interval was chosen as a compromise between retaining a large solar UV spectra dataset and

precision of the match with TOC. Due to the rapidly changing position of the polar vortex, the TOC values can vary greatly even within a relatively short time period. For example, a case study from the south Argentinean city Rio Gallegos by Orte et al. (2019) showed a drop in TOC by 70 DU in 24 hours, and Nichol and Valenti (1993) state that at South Pole, TOC may vary by more than 20 DU within several hours.

In order to express the effect of cloudiness, the ERA5 reanalysis data (Hersbach et al., 2020) were used. The spatial resolution was 0.25° × 0.25°, and the temporal resolution was 1 hour. This dataset was chosen due to the best correlation (r = 0.26) with the Marambio Base cloud modification factor (CMF, Park et al., 2017). CMF was calculated as the ratio between observed and clear-sky irradiance (e.g., Lindfors et al., 2007) for each wavelength, then the weighted mean using the clear-sky intensities as weights was derived for each spectrum. CMF was determined from the ground based spectral UV irradiance data from B199, and the theoretical clear-sky spectral UV irradiance was estimated using the one dimensional DISORT solver of the libRadtran radiative transfer package (Mayer and Kylling, 2005). TheThe input parameters in libRadtran were the day of year, SZA, B199 TOC, and albedo climatology (see further). CMF itself could not be paired with the UV spectra, as it was not independent of the studied variable.

The climatological albedo values for the Marambio Base location have been taken from the OMI surface UV algorithm (OMUVB) product of the NASA's Aura Ozone Monitoring Instrument, which provides surface albedo climatology at 360 nm (Tanskanen et al., 2006).), with the spatial resolution is 13 × 24 km at nadir. This dataset has only been used as an input to the UV irradiance model described in sect. 2.4.

2.4 Data Processing and Analysis

The data analyses were carried out for the solar spectra, as well as for the explanatory variables (SZA, TOC, cloudiness, albedo). At first, basic statistical characteristics were calculated for the entire period, individual months and seasons. Due to the non-normal distribution of the datasets, median was chosen as the preferred measure of central tendency, alongside with the use of nonparametric testing where applicable (e.g., Mann-Whitney U test and Kruskal-Wallis ANOVA, described in Kruskal and Wallis, 1952). All tests were performed at the significance level $\alpha = 0.05$.

In order to assess the change of UV irradiance over the study period, daily median spectra have been calculated, as well as their relative differences to the 2010–2020 median. The solar irradiances at 305 and 340 nm have been further emphasized. These wavelengths have been chosen because of their different absorption by ozone (Bernhard and Stierle, 2020), but also because the results could be easily compared with other studies (e.g., Bernhard et al., 2005, 2006; Diaz et al., 2006; or Stamnes et al., 1991). At these wavelengths, the distribution of very high values was studied as well. A very high value was defined as belonging in the top 10 % of all measured irradiances at the given wavelength.

The climatological effects of explanatory variables (SZA, TOC, and cloudiness, and albedo) were assessed using an artificial dataset built by an ANN model (see further in this section). Such model was preferred to a parametric multiple regression model (e.g., Antón et al., 2005) because according to DeVaux et al.,. (1993.), ANN models are suitable for noisy or

160   intercorrelated (Table 1) input data and to express nonlinear relationships. Moreover, no a-priori assumption on the dependency shape was needed.

Ten different ANN multilayer perceptron models were built, each with four inputs (SZA, TOC, cloudiness, and albedo) and 127 outputs (UV irradiance at the studied wavelengths in the interval 300.0–363.0 nm, with 0.5 nm resolution). Each time, the dataset was randomly divided into a training subset (70 % of the data), testing subset (15 %), and validation subset (15 %). At

165   the beginning of the training, each network was randomly initialized with a normal distribution with mean = 0 and standard deviation = 1. The stopping condition was set to the error improvement lower than 0.0000001 in the window of 200 cycles, while the error function was defined as the sum of squares.

Using the validation dataset, the performance of all ten models was assessed, (more information is included in Appendix A), and the best one was selected based on the absolute and relative bias, root mean square error (RMSE), and correlation with the

170   original data. According to the sensitivity analysis, SZA was the most important variable in the selected model, with the weight of 4.54, followed by cloud cover (1.14), TOC (1.05), and surface albedo (1.00).

However, even in the best of the ten models, a systematic bias was observed. So a correction was carried on: median bias values were calculated from the entire dataset separately for each wavelength and month, and then they were subtracted from the model output. The correction for medians tackled the systematic underestimation of UV irradiance at almost all

175   wavelengths (Fig. 3a,b). After the correction, 80 % of the data fitted between ±0.08 mW·m^{-2}. The relative differences were greater at very short wavelengths, but from approximately 310 nm, 80 % of the modelled data did not exceedwas within approximately ±25 %, which can also be seen in Fig. 3c. The correction improved the amount of data within ±1, 5, 10, and 25 %, in average by 0.5, 1.6, 2.0, and 1.5 %, respectively. The observations shareddetermination coefficient (R-squared, e.g. McClave and Dietrich, 1991) varied between 0.76 and 0.92 % of variability (Fig. 3d)., while R2it was greater at shorter

180   wavelengths., likely due to the smaller range of the data. The correction for medians increased the shared variabilityvariance, expressed by R-squared, in average by 0.1 %. RMSE was greater at longer wavelengths, and after the correction, it changed only within approximately ±0.0001 mW·m^{-2}.

After the best model was selected and the correction was performed, the effect of explanatory variables on the UV spectra was estimated. Out of the four explanatory variables, always justonly a single one was left to its original value, while the three

185   other variables were fixed to their monthly medians (Table 2). The use of individual months' medians was applied because neural networks generally present good results within the scope of the dataset, but they are not ideal for extrapolation, as they tend to overfit to the training dataset (e.g., Raksasat et al., 2021). So, modelingmodelling UV irradiance outside the dataset range, e.g., at a low SZA and very low TOC, could lead to very imprecise results. The breakdown of the dataset into individual months and the use of monthly medians prevented these inaccuracies, so it was possible to calculate the UV irradiance change

190   attributed to each of the four studied variables in the nine individual months.

Based on the above-described modeledmodelled data, the linearity and strength of the relationships were studied. At first, the relationships for each month at 305 and 340 nm were plotted, and then the mean absolute and relative change in spectral UV irradiance induced by the explanatory variables was assessed. The final part of the analysis consisted of several case studies,

where the ~~modeled~~modelled values were compared to the actual observed spectra, with the aim to compare the effect of one variable with the effect of all studied parameters. Each time, two spectra, one with a very high and the other with a very low value of a particular explanatory variable, were chosen, and the ~~observed and modeled spectra~~observations were compared with the modelled spectrum, where all variables except one were fixed to their monthly medians. Due to the difference of monthly median and the actual values, the ~~differences~~dissimilarities between the model and the observation showed also the combined effect of the other explanatory variables.

3 Results and Discussion

3.1 Solar UV spectra climatology and changes

Median solar UV irradiance generally increases with increasing wavelength~~.~~, but local minima exist at Fraunhofer lines and at wavelengths strongly absorbed in the Earth's atmosphere. Between 305 and 340 nm, the median UV irradiance increased approximately 25 times in summer and over 100 times in early spring and late fall. The difference is likely given by the effect of SZA, when in the high-SZA months, the solar UV ray path through the ozone layer is longer. The increase is faster in the UVB region, up to ~330 nm (Fig. 4a), where it makes in average 0.007 $\mathrm{mW \cdot m^{-2} \cdot nm^{-1}}$ but the shape is approximately exponential. At longer wavelengths, the increase changes to quasi-linear and slows down to 0.002 $\mathrm{mW \cdot m^{-2} \cdot nm^{-1}}$. This behavior is well represented in all months but due to the respective position of the Sun and the studied site, it is steeper in low-SZA months (Fig. 4b). This happens, again, because at low SZA, the atmospheric path is shorter, so less UV radiation is absorbed by ozone and other atmospheric gases. At shorter wavelengths (up to approx. 330 nm), the increase in median irradiance varies from 0.003 $\mathrm{mW \cdot m^{-2} \cdot nm^{-1}}$ in April to 0.010 $\mathrm{mW \cdot m^{-2} \cdot nm^{-1}}$ in December and January. At longer wavelengths, the irradiance variability increase is smaller and makes 0.001 $\mathrm{mW \cdot m^{-2} \cdot nm^{-1}}$ in August, September, March and April, and 0.002 $\mathrm{mW \cdot m^{-2} \cdot nm^{-1}}$ in other months. The precise shape of the spectrum, given by the extraterrestrial irradiance and atmospheric attenuation, remains similar in all months, with a higher variability between local maxima and minima in spring and autumn (effect of low SZA).

The relative differences of monthly medians to the overall median spectrum, which takes in account all observations from the 2010–2020 period, vary especially at wavelengths to about 320 nm (Fig. 4c). At 300 nm, the UV irradiance exceeds the overall median by up to 139 % in January and reaches only 7 % of it in April. However, at 363 nm, the monthly medians make up between 135 and 52 % of the overall one, so the difference is smaller. The change of the relative differences gradient in months affected by the ozone hole may be possibly attributed to the effect of variable ozone amount. In October, when the UV irradiance is lower than the overall median, the difference decreases with decreasing wavelengths, while in November, when the median irradiance already exceeds the overall median, the difference increases more steeply. The wave-like Huggins belt structure, visible in certain months, is likely also conditioned by the amount of ozone relative to the general central tendency (e.g., Gorshelev et al., 2014).

225 TOC (Fig. 4d) exhibits a pattern typical for Antarctic environment, i.e. depletion in austral spring, explained for example in Karhu et al. (2003) or Koo et al. (2018). In September, the median TOC value drops below the 220 DU level, while the absolute minimum, 113.7 DU, was recorded on 3 November 2015. In November and December, the median TOC values grow above the summer medians, which is likely due to the advection of subpolar, ozone rich air masses into the area of the decaying polar vortex. Over the study period, the highest TOC value was recorded on 6 November 2011, when it reached 402.0 DU. The

230 yearly cycle, as well as the short- and long-term fluctuations of TOC in the coastal Antarctic region are conditioned by both chemical and dynamical influences, while the chemical ones (like the catalytic reactions with the contribution of man-made chemicals) are now quite well understood (e.g., Solomon, 1999). The dynamical influences include the Brewer-Dobson circulation, which causes the poleward transport of ozone from the tropic to the poles, and subsequent accumulation of ozone in the polar regions in winter, as no UV radiation is present to induce ozone loss (Weber et al., 2011). Ozone depletion through

235 catalytic reactions starts in early spring and low TOC values are present till the breakdown of the polar vortex, which is caused by the dynamical effect of planetary waves and has much year-to-year variability (e.g., Shepherd, 2008), so it was possible to observe both the absolute ozone minimum and maximum in one month (November), only in different years. In Fig. 4d, the variability of TOC, which is much larger in spring than in any other season, is well visible.

The large variability of cloud cover at Marambio Base, with the median value of 68 % and mean of 59 %, is expressed in Fig.

240 4e. For the latitude of Marambio, Lachlan-Cope (2010)), who used latitudinal means obtained from satellite observations, presents a higher mean cloud cover (around 80 %). This difference is likely due to the position of Marambio at the eastern, i.e. leeward, and therefore less cloudy side of the Antarctic Peninsula. There is a hint of weak yearly cycle with maxima in September and minima in February, but the differences between the months are not statistically significant. In and therefore not conclusive. Based on satellite data, for the Antarctic Peninsula region, bothlocation of Marambio, all Adhikari et al. (2012),

245 Lachlan-Cope (2010) and Scott et al. (2017) found the cloud cover minima in winter and maxima in summer. However, due to the large cloud cover variability, mentioned also in Aun et al. (2020), the results presented in this study might have been affected by the choice of study period, and remain statistically not significant.

Median According to the surface albedo climatology, mean albedo at Marambio Base fluctuates between 0.42 in January and 0.61 in August (Fig. 4f).. Due to the snow cover melting and sea ice reduction, albedo decreases in the summer season, but in

250 March the sea ice recovers and albedo increases. Even though the differences between individual months are statistically significant again. However, albedo can occasionally approachexceed 0.8 even in summer months. This, which is likely related to snowfall events, becauseas at the Antarctic Peninsula, most precipitation falls in solid form, even though in summer, liquid precipitation can occur too (e.g., Ambrožová et al., 2020; Carrasco and Cordero, 2020; Engel et al., 2022).

The spectral UV irradiance represented in Fig. 5a shows a clear year to year variability with minima in early spring and late

255 autumn and maxima in Antarctic summer. However, the attenuation of UV irradiance in the atmosphere, caused likely by the action of clouds and atmospheric gases, frequently disrupts the dominant pattern. The lower intensity at some wavelengths (e.g., 316.5 nm or 358.5 nm), which is in Fig. 5a represented by the relatively darker vertical lines, has been caused by the presence of Fraunhofer absorption lines.

Although the absolute variability of UV irradiance is highest at the longer wavelengths, the relative variability (Fig. 5b) is greatest at the shortest wavelengths~~.~~, as seen from the presence of highest and lowest values of the ratio between the daily median spectra and the overall median (in Fig. 5b, where it is expressed on logarithmic scale). Also here, the minima occur in early spring and late autumn, but the maxima can be recorded both in summer and spring. This is further documented by Fig. 5c and 5e, which implies that at 305 nm, solar UV irradiance maxima can occur in October, as well as in December or January. For example, in the seasons 2010–2011 or 2017–2018 the summer (January) maximum, caused likely by low cloud cover, is more pronounced. However, in other seasons, such as in 2011–2012, 2014–2015 or 2018–2019, UV irradiance at 305 nm peaks in spring, particularly in October and November. The spring peak is affected mostly by ozone, which attenuates especially radiation of very short wavelengths (e.g., Bais et al., 1993; Gorshelev et al. 2014). Very short wavelengths seem to follow a similar pattern with a large, ozone-induced variability in spring at different locations in Antarctica, such as McMurdo Station (Bernhard et al., 2006), or Palmer Station (Bernhard et al., 2005), but also in the southernmost South America (Diaz et al., 2006). On the contrary, at 340 nm (Fig. 5d), the summer maximum is higher in all cases except the 2014–2015 season. This wavelength is considered largely unaffected by ozone, however, despite being affected much less than shorter wavelengths, in the cases of ~~large~~some deep ozone holes ~~(e.g., seasons 2013–2014 or 2014–2015),~~ irradiance increases can be seen even at longer wavelengths. This happened for example in seasons 2013–2014, the ozone hole was short-lasting but deep and well correlated with a drop in cloud cover, or in 2018–2019, where a drop in cloud cover was also observed.

~~Alongside atmospheric gases,~~Another parameter, important for the ~~surface~~ UV ~~irradiance~~radiation attenuation, is ~~also affected by the absorption in the troposphere, which is in this study represented by the~~ cloud cover. As seen from Table 2 and Fig. 4e, during the study period, maxima tend to occur in spring and minima in early fall, but there is much year to year variability (Fig. 5f). Near the Antarctic Peninsula, cloudiness can attenuate more than 90 % of UV irradiance, but in the case of a thin cloud cover and a short optical path through the atmosphere, this number can shrink to as little as 30 % (Lee et al., 2015). However, this amount is likely not the same at all wavelengths, as due to the increased scattering of shorter wavelengths in the atmosphere and thus the decreasing proportion of direct radiation (described e.g., in Schwander et al., 2002), clouds affect solar radiation at longer wavelengths more. Nevertheless, it seems that during cloudy days, such as in September 2010 or August to October 2017, UV irradiances at Marambio drop at both short and long wavelengths, while below-median cloudiness (e.g., December 2015) caused high summer UV irradiance peaks.

Surface properties, represented by albedo, ~~were found to be~~are another important factor affecting the spectral UV irradiance. Snow or sea ice can reflect 50 to 95 % of UV radiation, depending on SZA and surface quality, such as soot content. However, the ocean without sea ice only reflects 5–20 % of UV radiation, which may lead to its decline compared to snow cover or glaciated areas (Cordero et al., 2014; Zhou et al., 2019). Around Marambio Base, albedo reaches maxima at the end of winter (August to October), and minima in late summer (January to February). ~~This annual variation is quite steady with only little deviations from the climatological median (Fig. 5g), caused likely by snowfall events or, on the other hand, excessive snowmelt in the vicinity of Marambio Base.~~

Very high UV irradiances at Marambio Base at 305 and 340 nm, which were defined as the highest 10 % of all recorded values, were identified especially in spring and summer, typically from October to February (Fig. 6). Due to the effect of low ozone values, UV irradiance at 305 nm often peaks earlier than at 340 nm, and there are large differences between the number of high UV irradiances at 305 and 340 nm in each month. The two datasets only share less than 52 % of variability, ~~what~~which proves that it is important to study UV irradiance at separate wavelengths individually. For example, in October 2010, there were no high UV irradiances at 340 nm, but there were 34 of them at 305 nm. Although the ozone reduction in 2010 was relatively small (Fig. 5e, ~~de~~De Laat and ~~van~~Van Weele, 2011), relatively low cloudiness (median of 43 %, as seen in Fig. 5f) allowed the UV irradiance at 305 nm to reach very high values. Similarly, in the season 2011–2012, there were 12 cases of very high UV irradiances at 305 nm already in September and 84 of them in October, while there were only 3 cases at 340 nm in October 2011. In 2011, the ozone hole was relatively severe (Fig. 5e, Klekociuk et al., 2014), so it strongly affected the UV irradiance at 305 nm. Another similar example, where relatively deep and stable polar vortex with low ozone content increased the number of very high irradiance measurements at 305 nm but not at 340 nm, was the season 2018–2019 (Fig. 5e, and e.g., Klekociuk et al., 2021). On the contrary, in November 2017, only 18 cases of high UV irradiances were recorded at 305 nm, compared to 113 cases at 340 nm. This was due to very high TOC in November 2011 (the median value of TOC was 357.4 DU), which attenuated the solar irradiance at 305 nm.

3.2 Effects of explanatory variables on spectral UV irradiance

As seen from Fig. 7–10, the relationships between UV irradiance and explanatory variables, as ~~modeled~~modelled by the ANN model described in Section 2.4, are often not linear, and vary based on wavelength. The relationships and amounts of change for different months also vary, which demonstrates that they are affected by other variables. Therefore, Fig. 7–10 show examples of the relationships of the explanatory variables and UV irradiance, given that all other variables are fixed to their monthly medians.

Out of the four studied variables, SZA is the most important one affecting the UV irradiance at Marambio Base (Fig. 7). The relationship between UV irradiance and SZA at 305 nm (Fig. 7a) is not linear, as the increase in UV irradiance at lower SZA is faster than at high SZA values. Compared to other months, UV irradiance at 305 nm in September and October increases faster with the decrease in SZA, which is likely caused by its enhancements by the low TOC values in the ozone-hole period. The relationship between SZA and the ~~modeled~~modelled UV irradiance is getting ~~rather~~more linear with increasing wavelength (Fig. 7b), and the relative differences between individual months are smaller. The nonlinearity of the relationship can be explained by the solar UV irradiance being indirectly proportional to the cosine of SZA, and by the increasing absorption and scattering in the atmosphere as the optical path lengthens (e.g., Kerr and Fioletov, 2008). The absolute mean differences in UV irradiance for the 1° increase in SZA are greater at wavelengths longer than about 320 nm (Fig. 7c), but the relative changes are largest at the very short wavelengths (Fig. 7d). For example, at 340 nm, a 1° increase in SZA causes between 3 % decline in UV irradiance in December and 8 % in August, but at 305 nm, this change varies between 6 % in December and 18 % in March, provided all other variables are fixed to their monthly medians. Webb and Engelsen (2008) explain this by the

increasing path of UV radiation through the ~~ozonosphere~~atmospheric ozone layer, so the short wavelengths are attenuated more than the longer ones. The spectral dependence of the relationship between UV irradiance and SZA has also been shown in the case studies by Kerr and Fioletov (2008) or Tarasick et al. (2003), and indirectly also by the 340/305 nm ratio studied by Stamnes et al. (1991).

The fact that ozone affects UV irradiance more at shorter wavelengths can also be seen from Fig. 8. UV irradiance at 305 nm increases with the decrease in TOC (Fig. 8a) at an average rate of up to 0.002 mW·m^{-2} per 10 DU in November, but the relationship is nonlinear, with a faster increase at low TOC values. A similar, approximately exponential relationship of TOC and UV irradiance at 300 nm from South Argentina has been presented by Bojkov et al. (1995). The differences in the relationships between the studied months are likely caused by the effect of SZA, ~~as also~~ which is expressed in Fig. 7 or for example in Kerr ~~at al.~~and Fioletov (2008~~) observed a much steeper decline in UV irradiance at 300 nm in low-SZA conditions.~~).

At 340 nm, TOC is only a weak absorber of UV radiation (e.g., Gorshelev et al., 2014), so it does not have a profound effect at this wavelength (Fig. 8b). Nevertheless, in the low-SZA months, UV irradiance increases by up to 0.004 mW·m^{-2} in January with a 10DU decrease in ozone, though the relationship is nonlinear. The rather complex shape of the relationship is likely to be an artifact of the ANN model. The mean absolute change in UV irradiance induced by a 10DU increase in TOC is greatest at about 317.5 nm, ranging from -0.004 mW·m^{-2} in August to -0.006 mW·m^{-2} in January (Fig. 8c). On the contrary, the relative change is greatest at the shortest wavelengths, and it is getting close to 0 at the longer ones (Fig. 8d; also described in Bais et al., 1993). The Huggins belt wavy structure is clearly visible between approximately 315 and 335 nm. However, the shape of vertical ozone profile (e.g., Čížková et al., 2018) may play a substantial role in UV radiation absorption in the optical path, as different vertical distributions of ozone may lead to similar TOC values.

According to the ANN model, the effect of cloudiness (Fig. 9) seems to be generally quite weak at both 305 and 340 nm (Fig. 9a,b), being greater near the fully cloudy sky. The absolute change in spectral UV irradiance caused by a 10 % increase in cloud cover is greatest at the longer wavelengths (Fig. 9c), but the relative change is largest at the shortest wavelengths, especially in high-SZA months (Fig. 9d). However, from about 313 nm, the relative change of ~~modeled~~modelled UV irradiance remains almost the same, and it ranges from about -0.2 % in April to approximately -2.2 % in January. Although Bais et al. (1993) did not find any spectral dependence of the relationship between UV irradiance and cloud cover, Seckmeyer et al. (1996) and Kylling at al. (1997) argue that due to spectrally dependent Rayleigh scattering of UV radiation at top of cloud layer, the cloud transmittance is higher at shorter wavelengths. Similarly, Schwander et al. (2002) found that in the UVA region, the attenuation of UV radiation by clouds increases with increasing wavelength. The clouds can attenuate up to 99 % of UV radiation, however, their effect is generally weaker over the Antarctic continent, possibly explaining the relatively small changes detected by the ~~modeling~~modelling experiment. This happens because the Antarctic clouds are thinner than the ones in middle and low latitudes, affecting the portion of UV radiation penetrating through them (Calbó et al., 2005; Lubin and Frederick, 1991). Also Lee et al. (2015) show that in the Antarctic Peninsula region, the increase in cloud cover from clear sky to overcast causes only about 30 % decrease in erythemal UV irradiance, and this change is even smaller at high SZA. Similarly

to this study, they show a nonlinear relationship with a faster decline in erythemal UV irradiance when the cloud cover exceeds approximately 5 octas.

~~The last variable affecting UV irradiance, which is covered in this study, is surface albedo (Fig. 10). The relationship between albedo and UV irradiance is almost linear, although weak at both 305 and 340 nm (Fig. 10a,b). Generally, UV irradiance decreases with a decreasing albedo (~~In the last part of the study (Fig. 10), an assessment was carried out, looking at the effects of SZA, TOC, and cloud cover on the UV spectra on selected October days with extreme values of each parameter. The modelled results show the difference in UV spectra attributed to one selected variable in its high and low extremes, while all other parameters were fixed to their monthly medians. On the other hand, the dissimilarities between the model outputs and observations point out to the effect of all variables combined, which caused substantial differences between the real and modelled cases, where only one variable was altered from its monthly median.

~~Fig. 10c,d), while at wavelengths longer than 320 nm, a 0.1 change in albedo results in up to 1.5% increase in UV irradiance (in April). However, in other months, such as November, December and January, the albedo effect is not significant. According to the results of this study, at 320 nm, the change in albedo from 0.1 to 0.9 can lead to up to 26% increase in UV irradiance (in April). The change is greater in high-SZA months, which is in concordance with Lee et al. (2015). Cordero et al. (2014) state that albedo greater than 90 % can increase UV irradiance by up to 50 %, and Lee at al. (2015) say that the relative increase in UV irradiance on snow covered surfaces ranges between 15–30 %. However, since the albedo of different surfaces, including snow, is spectrally dependent (Wuttke et al., 2006) and the satellite data used in this study cover relatively large surface areas, the relationships described here can be seen as climatological, large-scale ones.~~

Looking at individual case studies featuring ~~a~~ solar ~~spectrum~~spectra measured at a high ~~SZA~~ and a ~~solar spectrum measured at a~~ low SZA (Fig. ~~11a~~10a), the ~~modeled~~modelled values confirm the relative ~~increase or decrease~~change of UV irradiance is greatest at the shortest wavelengths. However, ~~this is not the case in~~ the selected low-SZA ~~measurement~~case shows a dissimilarity between the model and the observation, as in the observed case, the short wavelengths ~~are~~were attenuated by a very high ozone content (about 120 DU higher than the monthly median~~, to which the model run was set)~~.). Therefore, it shows that the effect of SZA can be at least partly overrun by the effects of other explanatory variables~~.~~, as seen from Fig. 10a, where the anticipated increase of UV irradiance due to the effect of low SZA on 31 October 2012 was at wavelengths shorter than approximately 320 nm covered up by the ozone related attenuation.

The two ~~case studies~~cases from 28 October 2010 and 3 October 2011, presented in Fig. ~~11b~~10b, show models and measurements with ~~the~~ record-high and record-low October TOC, differing from each other by as much as 274 DU. The ~~modeled~~modelled UV irradiances are very close to the October median at wavelengths longer than about 320 nm, but at shorter wavelengths, the model irradiances deviate from each other~~.~~, clearly showing the effect of TOC. However, in the low-TOC case (3 October 2011), there is a dissimilarity between the model and observation, with the measured values being much lower than the modelled ones. This was caused by the effect of SZA, which was in reality more than 15° higher than in the model scenario. It shows that even at extremely low TOC conditions, ~~the~~ UV irradiance may not be record high due to other factors (e.g., SZA, cloudiness).

~~Fig.~~ ~~Therefore, the mismatch between the observed and modeled low-TOC irradiances can be explained by~~Fig. 10c represents the effect of ~~SZA, which was in reality more than 15° higher than the monthly median. The modeled values presented in Fig. 11c show~~cloudiness on 10 October 2010 and 3 October 2014. There is a ~~minor~~small difference between the modelled values in cases with 0 % and 100 % ~~cloud cover~~cloudiness, which is almost independent of the wavelength. ~~Similarly as in the previous cases, the ground-based observations differ from the model due to the effect of~~ The dissimilarity between the modelled and observed high cloudiness case shows the cloud cover effect being intensified by other variables, as both SZA and TOC were in reality higher than the monthly median used in the model. On the contrary, the explanatory ~~variables, most likely SZA. In the case of albedo, there is almost no difference between the modeled UV irradiances in the high and low albedo case (Fig. 11d), stating that the large-scale albedo as recorded by the satellites is the least important variable of the four covered by this study. The~~values in the low cloudiness case were similar to their monthly medians, resulting in a good agreement of the observations ~~differ from the models based on SZA, TOC, or even cloudiness, and due to the combination of these variables, the high-albedo case exhibits lower UV irradiances than the low-albedo case. However, in the long-term, albedo changes may become a more important factor affecting UV irradiance even on the regional scale. The Antarctic sea ice extent, which is the most important variable for the large-scale Antarctic Peninsula region albedo, is recently hitting record lows (e.g., Turner et al., 2022), so late summer to early fall UV irradiances may decrease. The absorbed solar radiation may then contribute to the sea ice – albedo positive feedback, causing even larger sea ice loss, with all its climatological consequences.~~and the model.

4 Summary and Conclusion

UV radiation is an important factor affecting the life on Earth, but its effects are spectrally dependent. However, in the southern polar areas, a detailed analysis of solar UV spectra and their response to different atmospheric and terrestrial factors was still missing. ~~This~~In this study ~~offers~~ a comprehensive analysis of spectral UV radiation, based on 10 years of Brewer spectrophotometer measurements, was carried out using the approach of neural network ~~modeling~~modelling. It helped to confirm the strongly wavelength-dependent ~~behavior~~behaviour of UV irradiance, showing the importance of spectral UV radiation assessment. The absolute differences between the UV irradiance spectra generally increase with increasing wavelength, but the relative differences are greater at the shortest wavelengths. In the studied months (August to April) at Marambio Base, the highest median UV irradiance was recorded in January (139 % of the overall median at 300 nm, 135 % at 363 nm), whereas the lowest one in April (7 % of the overall median at 300 nm, 52 % at 363 nm). However, in some seasons (e.g., 2011–2012, 2014–2015, 2018–2019), UV irradiance at the shortest studied wavelengths peaked in spring (October and November). The temporal distributions of very high UV irradiances at 305 and 340 nm only share less than 52 % of variability, showing that UV irradiances at different parts of the spectrum respond differently to the driving factors, such as SZA, TOC, or cloud cover ~~or surface albedo~~.

SZA is the most important variable affecting UV irradiance at Marambio Base. According to the ANN model, the increase in UV irradiance with the decrease in SZA is faster at short wavelengths, when at 305 nm, a 1° decline in SZA equals in average

between 6 and 18 % increase in UV irradiance, but only between 3 and 8 % at 340 nm, depending on the month. At Marambio Base, TOC shows a pattern typical for the southern polar conditions with a pronounced depletion in spring. Over the 2010–2020 period, the spring depletion was variable, with deep, long-lasting ozone holes in the seasons 2011–2012 or 2014 2015–2016. The absolute TOC minimum was reached on 3 November 2015. On the other hand, the 2019 ozone hole was the smallest on record. In seasons with a deep, long-lasting ozone hole, the spring peak of the UV irradiances at very short wavelengths is most visible. The relationship between TOC and UV irradiance at 305 nm is non-linear, with a faster increase at low TOC values. At this wavelength, a 10 DU increase in TOC causes a decrease in UV radiation, which totals, depending on the month, in average between 7 and 13 % decrease in UV irradiance.%. At 340 nm, TOC does not have a profound effect.

Due to the relatively thin Antarctic clouds, the effect of cloud cover on UV irradiance was found rather weak. The increase in cloud cover by 10 % caused between 1–2 % decrease in UV irradiance at both 305 and 340 nm, while the attenuation increased fastest between 90 % and 100 % cloudiness. Also the effect of satellite-based surface albedo was assessed as relatively weak, when a 0.1 increase in albedo represented only up to 2 % increase in UV irradiance at 320 nm and more.

Additional efforts are needed to extend this study by the evaluation of other variables, such as on-siteother atmospheric gases (tropospheric ozone or sulphur dioxide), the shape of vertical ozone profiles, but especially in-situ measured albedo, snow cover occurrence or the sea ice areaextent in a given perimeter around Marambio Base, because the albedo of different surfaces, including snow, is spectrally dependent. Similarly, cloud type may also be studied, as it is also an important variable affecting UV irradiance. Also it is important to note that the results of this study might have been influenced by the peculiar characteristics of the given location, so they cannot be easily applied to the entire Antarctic Peninsula region.

Appendix A

Artificial Neural Network model development and validation

Out of the ten ANN models we built, nine (ANN02 to ANN10) behaved in a similar way, while one (ANN01) was different, and showing the best performance confirmed by validation statistics. The differences between the models did not result from the ANN setting, which remained the same, but occurred due to the random initialization of the models and the random split of the dataset to training (70 %), testing (15 %), and validation (15 %) subsets. As seen from Fig. A1, the model ANN01 had the most data within ± 5, respective ± 10 % from observations, and it had the largest R-squared and lowest RMSE out of all ten models. However, the model was biased toward underestimation of UV irradiance throughout most of the spectrum. For the purpose of the study, it was best to choose a model with the best precision, i.e. the lowest variability of results, highest R-squared and lowest RMSE (model ANN01). Also, it was possible to tackle the bias present within the model using a simple median correction described in section 2.4.

Data availability

The solar radiation data used for the study are property of the Czech Hydrometeorological Institute, Hradec Králové, Czech
455 Republic and are the subject of the data policy of the above-mentioned institution. Any person interested in the underlying data should contact Ladislav Metelka, the head of the Solar and Ozone Observatory of the Czech Hydrometeorological Institute, Hradec Králové (email: ladislav.metelka@chmi.cz). The satellite and reanalyzed data courtesy of NASA and ECMWF, respectively.

Author contribution

460 K.Č., K.L. and L.M. designed the study, L.M. and M.S. provided the resources, L.M. and M.S. designed the ANN model and K.Č. validated it, K.Č. performed the data analyses and prepared the original manuscript draft, while K.L. and L.M. reviewed and edited it.

Competing interests

The authors declare that they have no conflict of interest.

465 **Special issue statement**

The work was presented online at the Quadrennial Ozone Symposium 2021 (poster No. SAT3_9) and we have expressed the interest to submit the paper to the joint Special Issue "Atmospheric ozone and related species in the early 2020s: latest results and trends" in ACP/AMT journals following on the QOS2021.

Acknowledgments

470 This research was supported by the State Environmental Fund of the Czech Republic, project of CHMI no. 03461022 'Monitoring of the ozone layer and UV radiation in Antarctica'; by the Czech Antarctic Research Programme 2022 (VAN 2022), funded by the Ministry of Education, Youth and Sports of the Czech Republic; and the project of Masaryk University (MUNI/A/1393/2021). The authors would like to thank the European Centre for Medium-Range Weather Forecasts for providing the ERA5 cloud cover data product and NASA AURA Validation Data Center for the surface albedo data
475 productsclimatology retrieved from OMI measurements. The authors are also grateful to the LAMBI laboratory and Marambio Base staff for operating the B199 Brewer spectrophotometer, namely to Janouch, M., Sieger, L., Brohart, M., Stráník, M., Hrabčák, P., Savastiouk, V, and Ochoa, H.

References

Adhikari, L., Wang, Z., and Deng, M.: Seasonal variations of Antarctic clouds observed by CloudSat and CALIPSO satellites, J. Geophys. Res., 117 (D04202), 1–17, 2012, DOI: 10.1029/2011JD016719.

Ambrožová, K., Hrbáček, F., and Láska, K.: The Summer Surface Energy Budget of the Ice-Free Area of Northern James Ross Island and Its Impact on the Ground Thermal Regime, Atmosphere-Basel, 11 (877), 1–18, 2020, DOI: 10.3390/atmos11080877.

Antón, M., Cancillo, M. L., Serrano, A., and García, J. A..: A Multiple Regression Analysis Between UV Radiation Measurements at Badajoz and Ozone, Reflectivity, and Aerosols Estimated by TOMS, Phys. Scripta, 118, 21–23, 2005.

~~Arola, A., Lakkala, K., Bais, A., Kaurola, J., Meleti, C., and Taalas, P.: Factors affecting short- and long-term changes of spectral UV irradiance at two European stations, J. Geophys. Res., 108 (D17), 1–9, 2003, DOI: 10.1029/2003JD003447.~~

Aun, M., Lakkala, K., Sanchez, R., Asmi, E., Nollas, F., Meinander, O., Sogacheva, L., De Bock, V., de Leeuw, G., Aaltonen, V., Bolsée, D., Cizkova, K., Mangold, A., Metelka, L., Jakobsen, E., Svendby, T., Gillotay, D., and Van Opstal, B.: Solar UV radiation measurements in Marambio, Antarctica, during years 2017–2019, Atmos. Chem. Phys., 20, 6037–6054, 2020.

Bais, A.: Absolute spectral measurements of direct solar ultraviolet irradiance with a Brewer spectrophotometer, Appl. Optics, 36, 5199–5204, 1997.

Bais, A., Zerefos, C. S., Meleti, C., Ziomas, I. C., and Tourpali, K.: Spectral Measurements of Solar UVB Radiation and its Relations to Total Ozone, SO2, and Clouds, J. Geophys. Res., 98 (D3), 5199–5204, 1993.

Barnes, P. W., Robson, T. M., Neale, P. J., Williamson, C. E., Zepp, R. G., Madronich, S., Wilson, S. R., Andrady, A. L., Heikkilä, A. M., Bernhard, G. H., Bais, A. F., Neale, R. E., Bornman, J. F., Jansen, M. A. K., Klekociuk, A. R., Martinez-Abaigar, J., Robinson, S. A., Wang, Q.-W., Banaszak, A. T., Häder, D.-P., Hylander, S., Rose, K. C., ~~Bernhard, G.: Trends of solar ultraviolet irradiance at Barrow, Alaska, and the effect of measurement uncertainties on trend detection, Atmos.~~ Wängberg, S.-Å., Foereid, B., Hou, W.-C., Ossola, R., Paul, N. D., Ukpebor, J. E., Andersen, M. P. S., Longstreth, J., Schikowski, T., Solomon, K. R., Sulzberger, B., Bruckman, L. S., Pandey, K. K., White, C. C., Zhu, L., Zhu, M., Aucamp, P. J., Liley, J. B., McKenzie, R. L., Berwick, M., Byrne, S. N., Hollestein, L. M., Lucas, R. M., Olsen, C. M., Rhodes, L. E., Yazar, S., and Young, A. R.: Environmental effects of stratospheric ozone depletion, UV radiation, and interactions with climate change: UNEP Environmental Effects Assessment Panel, Update 2021, Photochem. Photobiol. Sci., 21, 275–301, 2022.

~~Chem. Phys., 11, 13029–13045, 2011.~~

Bernhard, G., Booth, C., Ehramjian, J. C.: UV climatology at Palmer Station, Antarctica, based on Version 2 NSF network data, Proc. SPIE, 5886, 1–12, 2005, DOI: 10.1117/12.614172.

Bernhard, G., Booth, C. R., Ehramjian, J. C., and Nichol, S. E.: UV climatology at McMurdo Station, Antarctica, based on version 2 data of the National Science Foundation's Ultraviolet Radiation Monitoring Network, J. Geophys. Res., 111 (D11201), 1–15, 2006, DOI: 10.1029/2005JD005857.

Bernhard, G., and Stierle, S.: Trends of UV Radiation in Antarctica, Atmosphere-Basel, 11 (795), 1–26, 2020, DOI: 10.3390/atmos11080795.

Bognar, K., Ramina, A., Strong, K., Chipperfield, M. P., Dhomse, S. S., Drummond, J. R., Feng, W., Fioletov, V., Goutail, F., Herrera, B., Manney, G. L., McCullough, E. M., Millán, L. F., Pazmiño, A., Walker, K. A., Wizenberg, T., and Zhao, X.: Unprecedented Spring 2020 Ozone Depletion in the Context of 20 Years of Measurements at Eureka, Canada, J. Geophys. Res.-Atm., 126 (8), 2021, DOI: 10.1029/2020JD034365.

Bojkov, R. D., Fioletov, V. E., and Diaz, S. B.: The relationship between solar UV irradiance and total ozone from observations over southern Argentina, Geophys. Res. Lett., 22, 1249–1252, 1995.

Calbó, J., Pagès, D., and Gonzáles, J.-A.: Empirical studies of cloud effects on UV radiation: a review, Rev. Geophys., 43 (RG2002), 1–28, 2005, DOI: 10.1029/2004RG000155.

Carrasco, J. F. and Cordero, R. R.: Analyzing Precipitation Changes in the Northern Tip of the Antarctic Peninsula during the 1970–2019 Period, Atmosphere-Basel, 11 (1270), 1–19, 2020, DOI: 10.3390/atmos11121270.

Chubachi, S.: A Special Ozone Observation at Syowa Station, Antarctica from February 1982 to January 1983. In: Zerefos C.S., Ghazi A. (eds) Atmospheric Ozone. Springer, Dordrecht, 285–289, DOI: 10.1007/978-94-009-5313-0_58.

Čížková, K., Rieder, H. E., Staněk, M., Petropavlovskikh, I., Metelka, L., Láska, K.: Can Brewer Umkehr Measurements Capture Ozone Variability Near the Edge of the Southern Polar Vortex? Geophysical Research Abstracts, 20, EGU2018-2213, 2018.

Cordero, R. R., Seckmeyer, G., Pissulla, D., DaSilva, L., and Labbe, F.: Uncertainty evaluation of spectral UV irradiance measurements, Meas. Sci. Technol., 19 (045104), 1–15, 2008, DOI: 10.1088/0957-0233/19/4/045104.

Cordero, R. R., Damiani, A., Seckmeyer, G., Riechelmann, S., Labbe, F., Laroze, D., and Garate, F.: Satellite-derived UV climatology at Escudero Station, Antarctic Peninsula, Antarct. Sci., 25, 731–803, 2013.

Cordero, R. R., Damiani, A., Ferrer, J., Jorquera, J., Tobar, M., Labbe, F., Carrasco, J, and Laroze, D.: UV Irradiance and Albedo at Union Glacier Camp (Antarctica): A Case Study, PLOS ONE, 9 (e90705), 1–9, 2014, DOI: 10.1371/journal.pone.0090705.

Cordero, R. R., Damiani, A., Seckmeyer, G., Jorquera, J., Caballero, M., Rowe, P., Ferrer, J., Mubarak, R., Carrasco, J., Rondanelli, R., Matus, M., and Laroze, D.: The Solar Spectrum in the Atacama Desert, Sci. Rep.-UK, 6 (22457), 1–15, 2016, DOI: 10.1038/srep22457.

Cordero, R. R., Feron, S., Damiani, A., Redondas, A., Carrasco, J., Sepúlveda, E., Jorquera, J., Fernandoy, F., Llanillo, P., Rowe, P. M., and Seckmeyer, G.: Persistent extreme ultraviolet irradiance in Antarctica despite the ozone recovery onset, Sci. Rep.-UK, 12, 1–10, 2022, DOI: 10.1038/s41598-022-05449-8.

Czerwińska, A. and Krzyścin, J. W.: Climatological aspects of the increase of the skin cancer (melanoma) incidence rate in Europe, Int. J. Climatol., 40, 3196–3207, 2019.

De Laat, A. T. J~,~ and Van Weele, M.: The 2010 Antarctic ozone hole: Observed reduction in ozone destruction by minor sudden stratospheric warmings, Sci. Rep.-UK, 1 (38), 1–8, 2011, DOI: 10.1038/srep00038.

DeLuisi, J.: Atmospheric Ultraviolet Radiation Scattering and Absorption, NATO ASI Ser., 52, 65–84, 1997.

De Vaux, R. D., Psichogios, D. C., and Ungar, L. H.: A Comparison of Two Nonparametric Estimation Schemes: MARS and Neural Networks, Comput. Chem. Eng., 17, 819–837, 1993.

Diaz, S., Camilión, C., Deferrari, G., Fuenzalida, H., Armstrong, R., Booth, C., Paladini, A., Cabrera, S., Casicca, C., Lovengreen, C., Pedroni, J., Rosales, A., Zagarese, H., and Vernet, M.: Ozone and UV Radiation over Southern South America: Climatology and Anomalies, Photochem. Photobiol., 82, 834–843, 2006.

Diffey, B. L.: Ultraviolet radiation physics and the skin, Phys. Med. Biol., 25, 405–426, 1980.

Diffey, B. L.: Solar ultraviolet radiation effects on biological systems, Phys. Med. Biol., 36, 299–328, 1990.

Durbin, J., and Watson, G. S.: Testing for serial correlation in least squares regression I, Biometrika, 37, 409–428, 1950.

Farman, J. C., Gardiner, B. G., and Shanklin, J. D.: Large losses of total ozone in Antarctica reveal seasonal ClOx/NOx interaction, Nature, 315, 207–210, 1985.

Fitzka, M., Simic, S., and Hadzimustafic, J.: Long-term trends in spectral surface UV irradiance at Hoher Sonnblick (3106 m a.s.l.), AIP Conf. Proc., 1531, 776–779, 2013.

Glandorf, M., Arola, A., Bais, A., and Seckmeyer, Engel, Z., Láska, K., Kavan, J., and Smolíková, J.: Persistent mass loss of Triangular Glacier, James Ross Island, north-eastern Antarctic Peninsula, J. Glaciol., 1–13, 2022, DOI: 10.1017/jog.2022.42.

G.: Possibilities to detect trends in spectral UV irradiance, Theor. Appl. Climatol., 81, 33–44, 2005.

Gorshelev, V., Serdyuchenko, A., Weber, M., Chehade, W., and Burrows, J. P.: High spectral resolution ozone absorption cross-sections – Part 1: Measurements, data analysis and comparison with previous measurements around 293 K, Atmos. Meas. Tech., 7, 609–624, 2014.

Hersbach, H., Bell, B., Berrisford, P., Hirahara, S., Horányi, A., Muñoz-Sabater, J., Nicolas, J., Peubey, C., Radu, R., Schepers, D., Simmons, A., Soci, C., Abdalla, S., Abellan, X., Balsamo, G., Bechtold, P., Biavati, G., Bidlot, J., Bonavita, M., De Chiara, G., Dahlgren, P., Dee, D., Diamantakis, M., Dragani, R., Flemming, J., Forbes, R., Fuentes, M., Geer, A., Haimberger, L., Healy, S., Hogan, R. J., Hólm, E., Janisková, M., Keeley, S., Laloyaux, P., Lopez, P., Lupu, C., Radnoti, G., de Rosnay, P., Rozum, I., Vamborg, F., Villaume, S., and Tépaut, J.-N.: The ERA5 global reanalysis, Q. J. Roy. Meteor. Soc., 146, 1999–2049, 2020.

Holick, M. F.: Biological Effects of Sunlight, Ultraviolet Radiation, Visible Light, Infrared Radiation and Vitamin D for Helath, Anticancer Res., 36, 1345–1356, 2016.

Jovanović, Đ., Lukinović, M., and Vitošević, Z.: Environment and health – thirty years of successful implementation of the Montreal Protocol, Srp. Ark. Celok. Lek., 147, 492–496, 2019.

Juzeniene, A., Brekke, P., Dahlback, A., Andersson-Engels, S., Reichrath, J., Moan, K., Holick, M. F., Grant, W. B., and Moan, J.: Solar radiation and human health, Rep. Prog. Phys., 74, 1–56, 2011, DOI: 10.1088/0034-4885/74/6/066701.

Karhu, J. A., Taalas, P., Damski, J., and Kaurola, J.: Vertical distribution of ozone at Marambio, Antarctic Peninsula, during 1987–1999, J. Geophys. Res., 108 (D17, 4545), 1–9, 2003, DOI: 10.1029/2003JD001435.

580 Kerr, J. B. and Fioletov, V. E.: Surface Ultraviolet Radiation, Atmos. Ocean, 46, 159–184, 2008.

Klekociuk, A. R., Tully, M. B., Krummel, P. B., Gies, H. P., Petelina, S. V., Alexander, S. P., Deschamps, L. L., Fraser, P. J., Henderson, S. I., Javorniczky, J., Shanklin, J. D., Siddaway, J. M., and Stone, K. A.: The Antarctic ozone hole during 2011, Aust. Meteorol. Ocean., 64, 293–311, 2014.

Klekociuk, A. R., Tully, M. B., Krummel, P. B., Henderson, S. I., Smale, D., Querel, R., Nichol, S., Alexander, S. P.,
585 Fraser, P. J., and Nedoluha, G.: The Antarctic ozone hole during 2018 and 2019, J. South. Hemisphere Earth Syst. Sci., 71, 66–91, 2021.

Koo, J.-H., Choi, T., Lee, H., Kim, J., Ahn, D. H., Kim, J., Kim, Y.-H., Yoo, C., Hong, H., Moon, K.-J., and Lee, Y. G.: Total ozone characteristics associated with regional meteorology in West Antarctica, Atmos. Environ., 195, 78–88, 2018.

Kruskal, W. H., and Wallis, W. A.: Use of Ranks in One-Criterion Variance Analysis, J. Am. Stat. Assoc., 47, 583–621,
590 1952.

Kylling, A., Albold, A., and Seckmeyer, G.: Transmittance of a cloud is wavelength-dependent in the UV-range: Physical interpretation, Geophys. Res. Lett., 24, 397–400, 1997.

Lachlan-Cope, T.: Antarctic clouds, Polar Res., 29, 150–158, 2010.

Lakkala, K., Redondas, A., Meinander, O., Thölix, L., Hamari, B., Almansa, A.F., Carreno, V., García, R. D., Torres, C.,
595 Deferrari, G., Ochoa, H., Bernhard, G., Sanchez, R. and de Leeuw, G.: UV measurements at Marambio and Ushuaia during 2000–2010, Atmos. Chem. Phys., 18, 16019–16031, 2018.

Lakkala, K., Aun, M., Sanchez, R., Bernhard, G., Asmi, E., Meinander, O., Nollas, F., Hülsen, G., Aaltonen, V., Arola, A, and de Leeuw, G.: New continuous total ozone, UV, VIS and PAR measurements at Marambio, 64°S, Antarctica, Earth Syst. Sci. Data, 12, 947–960, 2020.

600 Lee, Y. G., Koo, J.-H., and Kim, J.: Influence of cloud fraction and snow cover to the variation of surface UV radiation at King Sejong station, Antarctica, Atmos. Res., 164–165, 99–109, 2015.

Lindfors, A., Kaurola, J., Arola, A., Koskela, T., Lakkala, K., Josefsson, W., Olseth, J. A., and Johnsen, B.: A method for reconstruction of past UV radiation based on radiative transfer modelling: Applied to four stations in northern Europe, J. Geophys. Res., 112 (D23201), 1–15, 2007, DOI: doi:10.1029/2007JD008454.

605 Lubin, D. and Frederick, J. E.: The Ultraviolet Environment of the Antarctic Peninsula: The Roles of Ozone and Cloud Cover, J. Appl. Meteorol., 30, 478–493, 1991.

Mayer, B. and Kylling, A.: Technical note: The libRadtran software package for radiative transfer calculations – description and examples of use, Atmos. Chem. Phys., 5, 1855–1877, 2005.

McClave, J. T. and Dietrich, F. H.: Statistics, San Francisco, CA: Dellon Publishing Company, 928 p., 1991.

610   McKenzie, R., Kotkamp, M., Seckmeyer, G., Erb, R., Roy, C. R., Gies, H. P., and Toomey, S. J.: First Southern Hemisphere Intercomparison of Measured Solar UV Spectra, Geophys. Res. Lett., 20, 2223–2226, 1993.

McKenzie, R., Aucamp, P. J., Bais, A. F., Björn, L. O., and Ilyas, M.: Changes in biologically-active ultraviolet radiation reaching the Earth's surface, Photochem. Photobiol. Sci., 2007, 218–231, 2007.

McKenzie, R., Bernhard, G., Liley, B., Disterhoft, P., Rhodes, S., Bais, A., Morgenstern, O., Newman, P., Oman, L.,
615   Brogniez, C., and Simic, S.: Success of Montreal Protocol Demonstrated by Comparing High-Quality UV Measurements with "World Avoided" Calculations from Two Chemistry-Climate Models, Sci. Rep.-UK, 9, 1–13, 2019, DOI.: 10.1038/s41598-019-48625-z.

Meinander, O., Josefsson, W., Kaurola, J., Koskela, T., and Lakkala, K.: Spike detection and correction in Brewer spectroradiometer ultraviolet spectra, Opt. Eng., 42, 1812–1819, 2003.

620   Nichol, S. E. and Valenti, C.: Intercomparison of total ozone measured at low sun angles by the Brewer and Dobson spectrophotometers at Scott Base, Antarctica, Geophys. Res. Let., 20, 2051–2054, 1993.

Orte, P. F., Wolfram, E., Salvador, J., Mizuno, A., Bègue, N., Bencherif, H., Bali, J. L., D'Elia, R., Pazmiño, A., Godin-Beekmann, S., Ohyama, H., and Quiroga, J.: Analysis of a southern sub-polar short-term ozone variation event using a millimeter-wave radiometer, Ann. Geophys., 37, 613–629, 2019.

625   Park, S. S., Kim, M., Lee, H., Lee, H., Kim, S.-M., and Lee, Y. G..: Estimating Cloud and Aerosol UV Modification Factors Based on Spectral Measurement from the Brewer Spectrophotometer, Atmosphere-Basel, 8 (109), 1–17, 2017, DOI: 10.3390/atmos8060109.

Pazmiño, A., Godin-Beekmann, S., Ginzburk, M., Bekki, S., Hauchecorne, A., Piacentini, R. D., and Quel, E. J.: Impact of Antarctic polar vortex occurrences on total ozone and UVB radiation at southern Argentinean and Antarctic stations
630   during 1997–2003 period, J. Geophys. Res., 110 (D03103), 1–13, 2005, DOI: 10.1029/2004JD005304.

Pazmiño, A., Godin-Beekman, GS., Hauchecorne, A., Claud, C., Khaykin, S., Goutail, F., Wolfram, E., Salvador, J., and Quel, E.: Multiple symptoms of total ozone recovery inside the Antarctic vortex during Austral spring, Atmos. Chem. Phys., 18, 7557–7572, 2018.

Petkov, B. H., Láska, K., Vitale, V., Lanconelli, C., Lupi, A., Mazzola, M., and Budíková, M.: Variability in solar
635   irradiance observed at two contrasting Antarctic sites, Atmos. Res., 172–173, 126–135, 2016.

Qu, Z.-W., Zhu, H., Grebenshchikov, S. Y., Schinke, R., and Farantos, S. C.: The Huggins band of ozone: A theoretical analysis, J. Chem. Phys., 121, 11731–11745, 2004.

Raksasat, R., Sri-iesaranusorn, P., Pemcharoen, J., Laiwarin, P., Buntoung, S., Janjai, S., Boontaveeyuwat, E., Asawanonda, P., Sriswasdi, S., and Chuangsuwanich, E.: Accurate surface ultraviolet radiation forecasting for clinical
640   applications with deep neural network, Sci. Rep.-UK, 11 (5031), 1–12, 2021, DOI: 1038/s41598-021-84396-2.

Scarnato, B., Staehlin, J., Stübl, R, and Schill, H.: Long-term total ozone observations at Arosa (Switzerland) with Dobson and Brewer instruments (1988–2007), J. Geophys. Res., 115 (D13306), 1–11, 2010, DOI: 10.1029/2009JD011908.

Schwander, H., Koepke, P., Kaifel, A., and Seckmeyer, G.: Modification of spectral UV irradiance by clouds, J. Geophys. Res., 107 (D16), 1–12, 2002, DOI: 10.1029/2001JD001297.

645 Scott, R., Lubin, D., Vogelman, A. M., and Kato, S.: West Antarctic Ice Sheet Cloud Cover and Surface Radiation Budget from NASA A-Train Satellites, J. Climate, 30, 6151–6170, 2017.

Seckmeyer, G., Erb, R., and Albold, A.: Transmitance of a cloud is wavelength-dependent in the UV-range, Geophys. Res. Lett., 23, 2753–2755, 1996.

Shepherd, T. G.: Dynamics, Stratospheric Ozone, and Climate Change, Atmos. Ocean, 46, 117–138, 2008.

650 Solomon, S.: Stratospheric ozone depletion: a review of concepts and history, Rev. Geophys., 37, 275–316, 1999.

Solomon, S., Ivy, D. J., Kinnison, D., Mills, M. J., Neely, R. R., and Schmidt, A.: Emergence of healing in the Antarctic ozone layer, Science, 353, 269–274, 2016.

Stair, R.: Ultraviolet Spectral Distribution of Radiant Energy From the Sun, J. Res. Nat. Bur. Stand., 46, 353–357, 1951.

Stamnes, K., Slusser, J., and Bowen, M.: Derivation of total ozone abundance and cloud effects from spectral irradiance 655 measurements, Appl. Optics, 30, 4418–4426, 1991.

Tanskanen, A., Krotkov, N. A., Herman, J. R., and Arola, A.: Surface Ultraviolet Irradiance from OMI, IEEE T. Geosci. Remote, 44, 1267–1271, 2006.

Tarasick, D. W., Fioletov, V. E., Wardle, D. I., Kerr, J. B., McArthur, L. J. B., and McLinden, C. A.: Climatology and trends of surface UV radiation, Atmos. Ocean, 41, 121–138, 2003.

660 Turner, J., Holmes, C., Harrison, T. C., Phillips, T., Jena, B., Reeves-Francois, T., Fogt, R., Thomas, E. R., and Bajish, C. C.: Record Low Antarctic Sea Ice Cover in February 2022, Geophys. Res. Lett., 49 (12), 1–11, DOI: 10.1029/2022GL098904.

UNEP: Environmental effects of ozone depletion and its interaction with climate change: 2010 assessment, United Nations Environment Programme (UNEP), Nairobi, 278, 2010.

665 Webb, A. R.: Ultraviolet radiation: the missing link in the ozone debate, Norsk Geol. Tidsskr., 71, 211–213, 1991.

Webb, A. R. and Engelsen, O.: Ultraviolet Exposure Scenarios: Risks of Erythema from Recommendations on Cutaneous Vitamin D Synthesis, Adv. Exp. Med. Biol., 624, 72–85, 2008.

Weber, M., Dikty, S., Burrows, J. P., Garny, H., Dameris, M., Kubin, A., Abalichin, J., and Langematz, U.: The Brewer-Dobson circulation and total ozone from seasonal to decadal time scales, Atmos. Chem. Wuttke, S., Seckmeyer, G., and 670 König-Langlo, G.: Measurements of spectral snow albedo at Neumayer, Antarctica, Ann. Geophys., 24, 7–21, 2006. Phys., 11, 11221–11235, 2011.

Young, A. R., Morgan, K. A., Harrison, G. I., Lawrence, K. P., Petersen, B., Wulf, H. C., and Philipsen, P. A.: A revised action spectrum for vitamin D synthesis by suberythemal UV radiation exposure in humans in vivo, PNAS, 118 (e2015867118), 1–8, 2021, DOI: 10.1073/pnas.2015867118.

675 Zhou, C., Zhang, T., and Zheng, L.: The Characteristics of Surface Albedo Change Trends over the Antarctic Sea Ice Region during Recent Decades, Remote Sens.-Basel, 11 (821), 1–25, 2019, DOI: 10.3390/rs11070821.

Table 1: Intercorrelation of explanatory variables (SZA = solar zenith angle; TOC = total ozone column; CLD = cloudiness; ALB = albedo). Statistically significant results (α = 0.05) are marked with an asterisk.

	SZA	TOC	CLD
TOC	-0.23*	·	·
CLD	-0.04*	-0.12*	·
ALB	0.20*	-0.19*	-0.01

680

Table 2: Monthly median values of explanatory variables (SZA = solar zenith angle; TOC = total ozone column; CLD = cloudiness; ALB = albedo) at Marambio Base in 2010–2020, which were used to fix the variables in the ANN model runs.

	AUG	SEP	OCT	NOV	DEC	JAN	FEB	MAR	APR
SZA	76.11	70.13	61.75	55.60	52.12	53.50	59.27	67.12	74.59
TOC	246.5	205.5	223.7	300.2	311.4	287.8	283.7	273.6	283.0
CLD	67	76	73	70	66	64	62	67	71
ALB	0.61	0.60	0.62	0.57	0.47	0.42	0.43	0.51	0.59

685
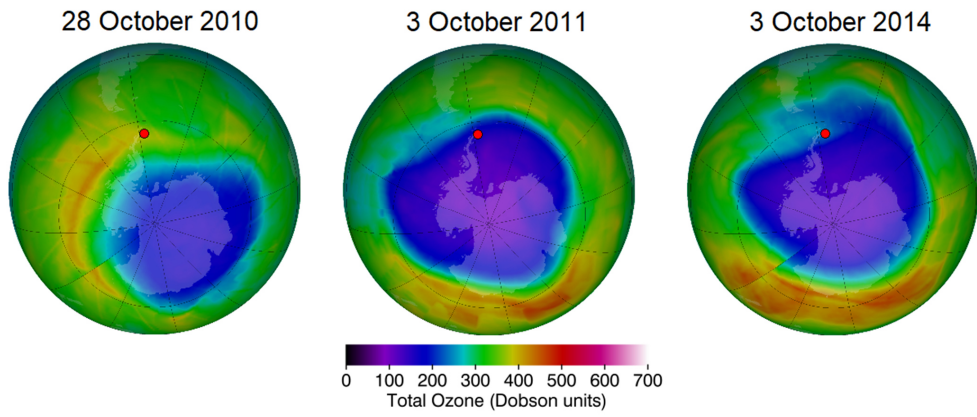
Figure 1: The approximate position of Marambio Base (red dot) relative to the southern polar vortex (outside, inside, and on the edge) on different October days. Image adapted from Ozone Hole Watch (2022).
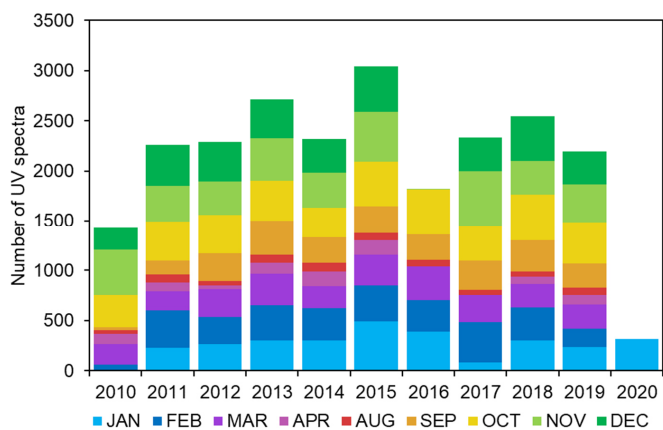
690

Figure 2: Number of solar UV spectra used in this study measured by the B199 Brewer spectrophotometer at Marambio Base over the period 2010–2020.
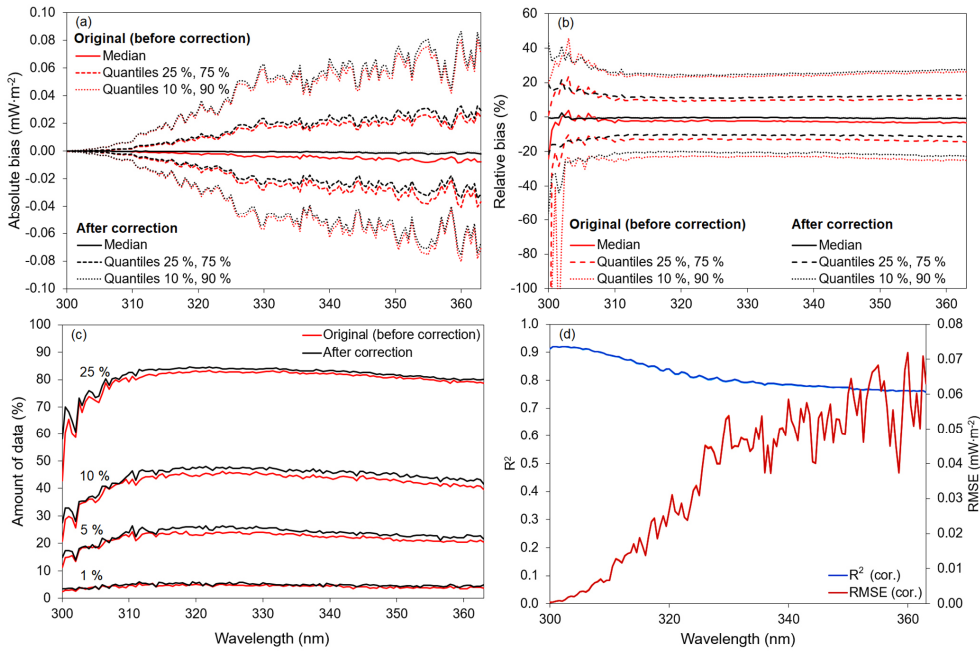
695   Figure 3: Validation of the ANN model before and after the median correction, while (a) represents the absolute bias quantiles, (b) are the relative bias quantiles, (c) is the amount of data within 1, 5, 10, and 25 % from observations, and (d) is the ~~R2~~R-squared and RMSE.

Commented [KC1]: Albedo panel removed
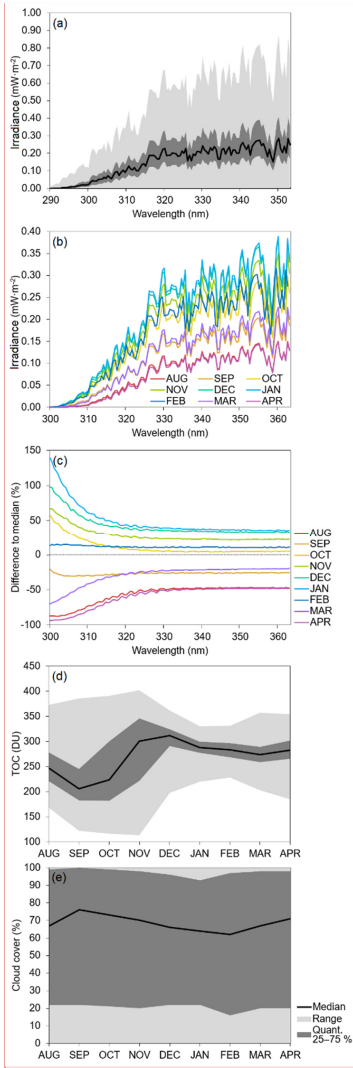
700   **Figure 4: Observed solar UV spectra and variables related to them obtained at Marambio Base in 2010–2020, while (a) represents statistical characteristics of all spectra, (b) monthly medians, and (c) relative differences of monthly medians to overall median, and (d), (c) and (fe) show the climatology of TOC, and cloud cover, and surface albedo, respectively.**
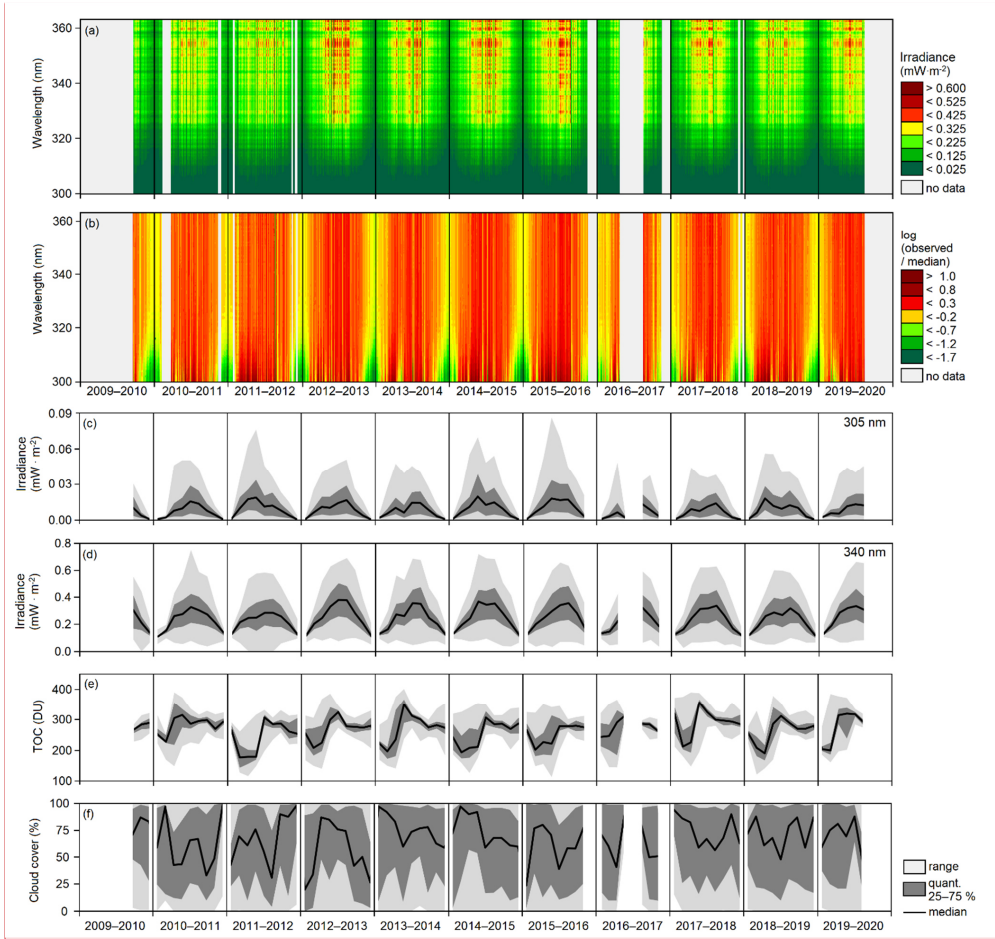
Commented [KC2]: Albedo panel removed

Figure 5: UV irradiance and related variables at Marambio Base over the period 2010–2020, while (a) represents the daily median intensities of spectral UV irradiance, (b) the daily median spectral UV irradiances relative to the overall median, on logarithmic scale, at a given wavelength, (c) the monthly variability of solar irradiance at 305 nm, (d) the monthly variability of solar irradiance at 340 nm, (e) the monthly variability of TOC, and (f) the monthly variability of cloud cover, and (g) the monthly variability of albedo.
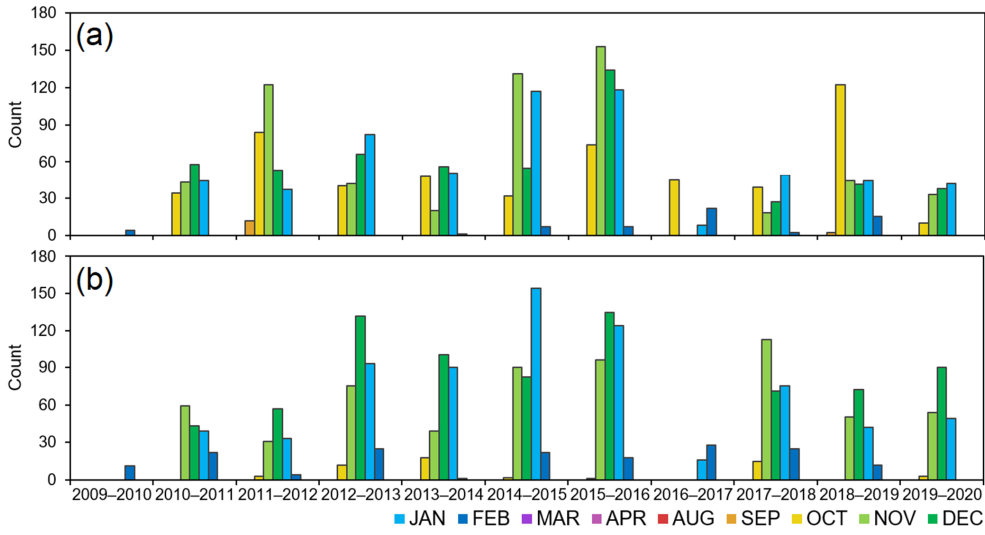
710   **Figure 6: Monthly distribution of the 10 % highest UV irradiances at (a) 305 nm, and (b) 340 nm, at Marambio Base, 2010–2020.**
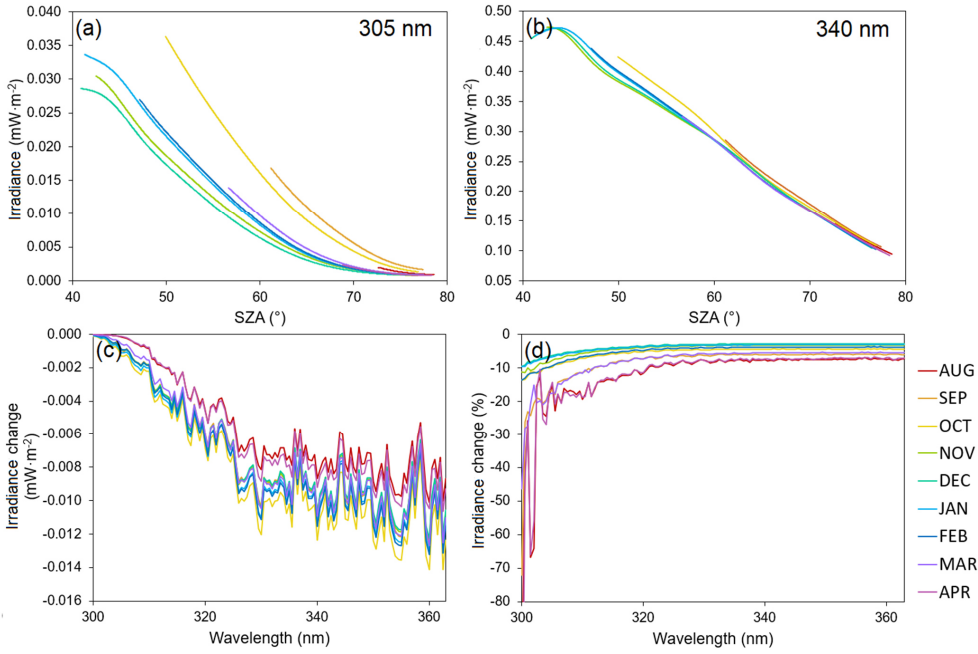
Figure 7: ~~Modeled~~Modelled relationships between UV irradiance and SZA for individual months, and mean absolute and relative changes in spectral UV irradiance caused by SZA change, while (a) and (b) represent the ~~modeled~~modelled SZA effect at 305 and 340 nm, respectively, (c) and (d) modelled mean absolute and relative change in spectral UV irradiance induced by a 1° increase in SZA~~.~~, while the relative changes were calculated with reference to the monthly median spectra.
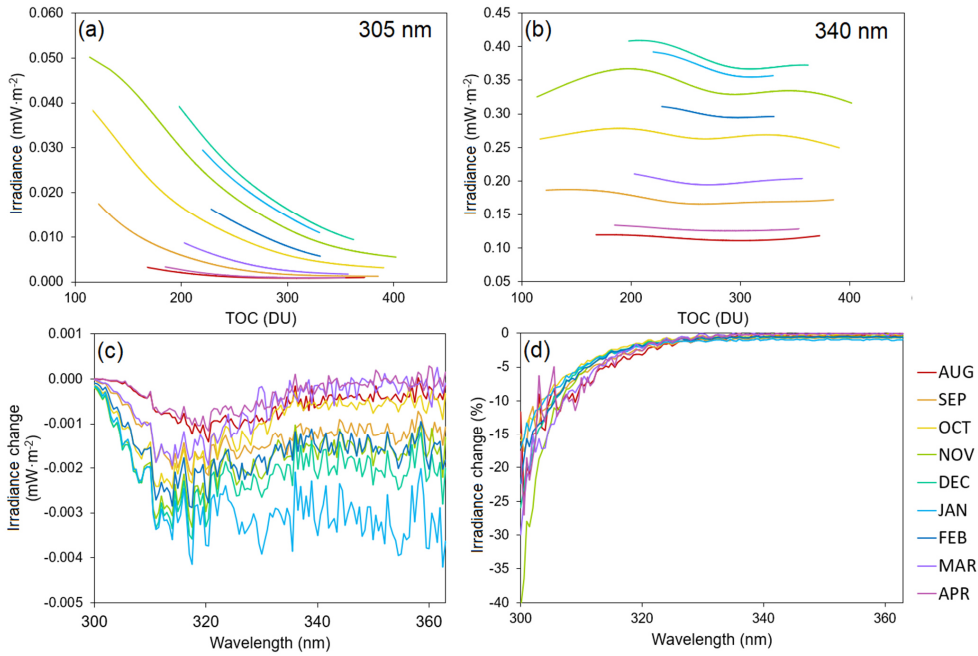
Figure 8: ~~Modeled~~Modelled relationships between UV irradiance and TOC for individual months, and mean absolute and relative changes in spectral UV irradiance caused by TOC change, while (a) and (b) represent the ~~modeled~~modelled TOC effect at 305 and 340 nm, respectively, (c) and (d) modelled mean absolute and relative change in spectral UV irradiance induced by a 10 DU increase in TOC, while the relative changes were calculated with reference to the monthly median spectra.
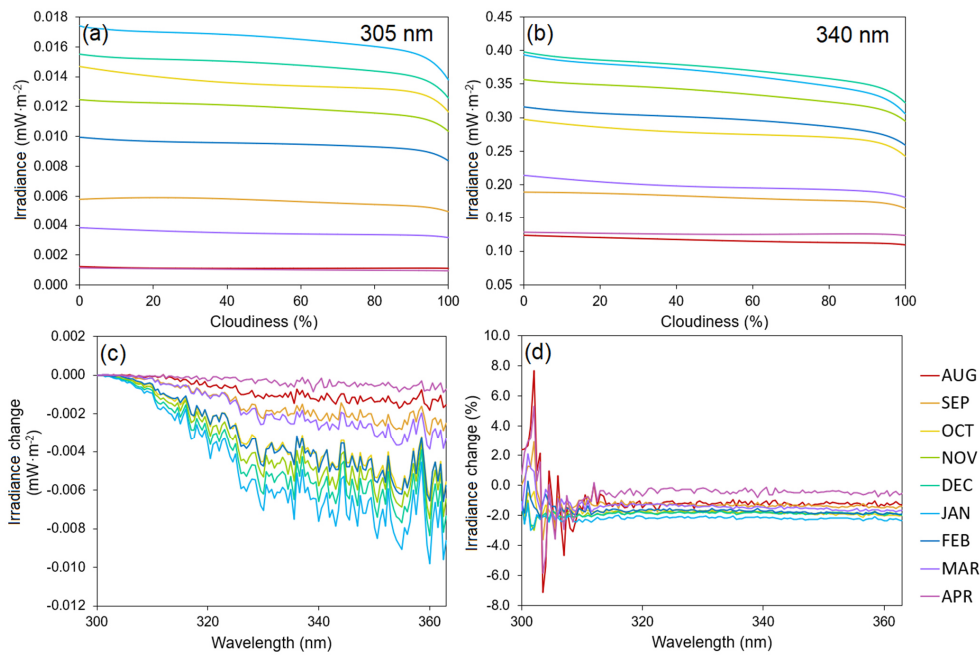
Figure 9: ~~Modeled~~Modelled relationships between UV irradiance and cloudiness for individual months, and mean absolute and relative changes in spectral UV irradiance caused by the change in cloudiness, while (a) and (b) represent the ~~modeled~~modelled effect of cloudiness at 305 and 340 nm, respectively, (c) and (d) modelled mean absolute and relative change in spectral UV irradiance induced by a 10 % increase in cloudiness, while the relative changes were calculated with reference to the monthly median spectra.
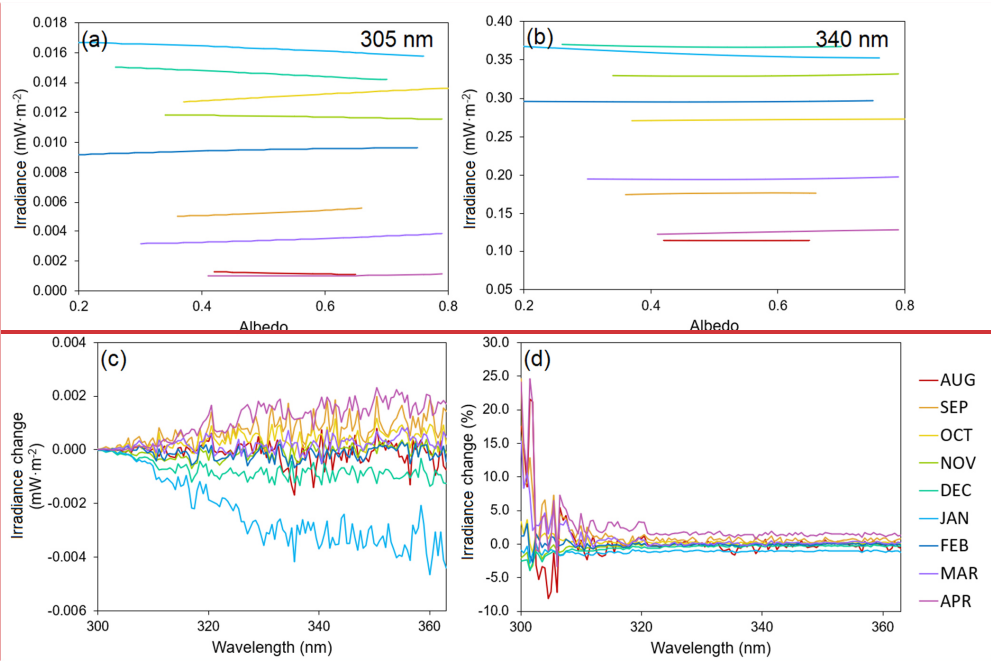
730

Figure 10: Modeled relationships between UV irradiance and surface albedo for individual months, and absolute and relative changes in spectral UV irradiance caused the change in albedo, while (a) and (b) represent the modeled effect of albedo at 305 and 340 nm, respectively, (c) and (d) absolute and relative change in spectral UV irradiance induced by the increase in albedo by 0.1.

	Obs.	Mod.
High SZA 7 October 2016, 20:03		
SZA (°)	75.01	75.01
TOC (DU)	244.0	223.7
Cld. (%)	8	73
Alb.	0.38	0.62

	Obs.	Mod.
Low SZA 31 October 2012, 15:33		
SZA (°)	49.90	49.90
TOC (DU)	343.2	223.7
Cld. (%)	94	73
Alb.	0.64	0.62

	Obs.	Mod.
High TOC 28 October 2010, 18:03		
SZA (°)	57.47	61.75
TOC (DU)	390.6	390.6
Cld. (%)	24	73
Alb.	0.64	0.62

	Obs.	Mod.
Low TOC 3 October 2011, 20:03		
SZA (°)	76.53	61.75
TOC (DU)	116.6	116.6
Cld. (%)	0	73
Alb.	0.60	0.62

	Obs.	Mod.
High cloudiness 18 October 2010, 12:33		
SZA (°)	62.80	61.75
TOC (DU)	223.2	223.7
Cld. (%)	100	100
Alb.	0.65	0.62

	Obs.	Mod.
Low cloudiness 3 October 2014, 14:03		
SZA (°)	62.43	61.75
TOC (DU)	235.4	223.7
Cld. (%)	0	0
Alb.	0.60	0.62

— High (obs.) − − − High (mod.)
— Low (obs.) − − − Low (mod.)

Figure 10: Spectral UV irradiance intensity relative to the monthly median on eight selected October days with extremely high or low (a) SZA, (b) TOC, ~~(c) cloudiness, and (d) albedo at Marambio Base in 2010–2020.~~ and (c) cloudiness at Marambio Base in 2010–2020. The dissimilarities between the model output, where three out of four explanatory variables were set to their monthly median, and the actual observation, shows the combined impact of the three variables that were set to their medians in the model and whose values are shown in the tables on the right.

Commented [KC4]: Albedo panel removed

745